Ultrastrong Field Ionization of Ne^{n+} ($n \leq 8$): Rescattering and the Role of the Magnetic Field

S. Palaniyappan, A. DiChiara, E. Chowdhury, A. Falkowski, G. Ongadi, E. L. Huskins, and B. C. Walker

Physics and Astronomy Department, University of Delaware, Newark, Delaware 19716, USA

(Received 21 October 2004; published 22 June 2005)

Ne^{+} to Ne^{8+} ionization yields in 10^{14} W/cm^2 to 10^{18} W/cm^2 laser fields are reported over a 10^9 dynamic range. A 3D relativistic rescattering model incorporating $(e, 2e)$ and $(e, 3e)$ electron impact ionization, single- and double-excitation is compared to the data. For double ionization the agreement is excellent; however, for higher charge states the model accounts for only 15% of multielectron nonsequential ionization. Rescattering is not affected by the laser magnetic field until 10^{17} W/cm^2.

DOI: 10.1103/PhysRevLett.94.243003 PACS numbers: 32.80.Rm, 31.90.+s, 32.80.Fb

Atomic ionization and radiation processes in strong fields have remained at the forefront of time resolved dynamics and laser science for the past 15 years. Recent interest has focused on quantum [1] and classical mechanisms [2] behind multielectron, multiphoton ionization and the new area of attosecond science [3,4]. These studies, which often address multielectron nonsequential ionization (NSI) [5] and high harmonic generation (HHG) [6], involve a field driven rescattering mechanism. As the field increases, higher charge states, relativistic effects, and the laser magnetic field ($\mathbf{B}_{\text{laser}}$) will affect NSI, HHG, and rescattering physics. This Letter begins to address these topics with a precision, ultrahigh field ionization experiment and relativistic, semiclassical ionization and rescattering model.

Rescattering [7] occurs when a photoelectron, which is oscillating in the continuum with the laser electric field ($\mathbf{E}_{\text{laser}}$), is driven back toward the parent ion. For laser intensities from 10^{13} W/cm^2 to 10^{15} W/cm^2, inelastic rescattering between the photoelectron and the parent ion may result in collisional ionization (NSI) or radiation (HHG). Two-electron NSI has been observed [8] to exceed by 10^5 the expected doubly ionized species from a sequential ionization (SI) mechanism, in which the laser field ionizes the atom one electron at a time. Recent theoretical [9–12] and experimental efforts have made significant progress towards understanding two-electron NSI mechanisms including resonantly enhanced multiphoton ionization [13,14] and rescattering impact excitation and ionization [15].

Beyond two-electron NSI of the neutral atom, multielectron NSI has been reported [16] but is not well understood at this time. Fully differential rates for the multiphoton ionization of ground state Ne [17], correlated electron emission measurements for multiphoton double ionization [18], and ion momentum measurements [19] indicate rescattering is likely to become a dominant NSI mechanism in ultrahigh fields with high charge states. Chowdhury [20] and Dammasch [21] measured multielectron ionization from 10^{15} W/cm^2 to $>10^{17}$ W/cm^2 and found NSI decreased at higher intensities. Diminished NSI was at first believed to result from a reduction in rescattering due to the Lorentz force on the photoelectron. In the "Lorentz force paradigm," $\mathbf{B}_{\text{laser}}$ and the significant photoelectron velocity force the rescattering into the laser propagation direction ($\hat{k} = \hat{v} \times \hat{B}$) and away from the parent ion. As we will show, $\mathbf{B}_{\text{laser}}$ does not play as large of a role as previously expected and there are outstanding questions on the mechanisms behind rescattering and ionization in the ultrahigh intensity regime.

This Letter presents experimental and theoretical results on Ne ionization in the nonrelativistic strong field ($v/c \cong 0$ and $\vec{p} \cdot \vec{k} = 0$ for the photoelectron) and ultrastrong field regime ($v/c \neq 0$ and $\vec{p} \cdot \vec{k} \neq 0$). The division between these two regimes occurs at about one atomic unit for the laser field (3×10^{16} W/cm^2). Though our model and data agree for Ne double ionization, a discrepancy with high charge states indicates an additional mechanism is present involving doubly excited states. We show the Lorentz force is important only as the intensity reaches 10^{17} W/cm^2.

The experimental apparatus consisted of a chirped pulse regenerative amplifier, a terawatt multipass amplifier and a time-of-flight ion spectrometer. A regenerative amplifier gave a 5.5 mJ output with 1.6% energy fluctuations at a repetition rate from 10 to 1000 Hz [22] and created intensities up to 10^{17} W/cm^2. The terawatt multipass amplifier (10 Hz) created intensities up to 10^{18} W/cm^2 and produced 250 mJ with 4.5% energy fluctuations. The laser pulse was 40 ± 5 fs in duration, had a center wavelength of 780 nm and a TEM_{00} [23] spatial mode. A $f/2$ off-axis parabola in vacuum focused the laser into an effusive Ne beam. The ion spectrometer analyzed the ions every shot. The intensity dependent ionization of the Ne valence shell is shown in Fig. 1. The data is averaged into 10% intensity bins; typically each data point represents three independent, million shot collections. The laser intensity is calibrated to an accuracy of 50% with linearity better than 20%. The ion signal error bars are estimated to be a factor of 2. Fluctuations in the ion yield between collections are shown in Fig. 1 for several data points.

The SI component of the yield is calculated here using a tunneling ionization model by Ammosov, Delone and Krainov (ADK) [24]. Briefly, ADK is the nonrelativistic field ionization rate of the outermost electron in an atom or

ion by tunneling through the Coulomb barrier suppressed by $\mathbf{E}_{\text{laser}}$. The SI yield, obtained by spatially and temporally integrating the ADK rate over the experimental pulse, is shown in Fig. 1. ADK and our measurements agree for yields from 10^4 ions/(shot torr) to 10^8 ions/(shot torr). For Ne^{7+} and Ne^{8+} the data agrees with ADK over the full experimental dynamic range. Small fluctuations in the curves above ionization saturation—i.e., Ne^{3+} and Ne^{8+} yields $>10^6$ ions/(shot torr)—are within the measurement uncertainty. Ionization yields for Ne^{5+} are measured with $^{22}Ne^{5+}$ to avoid $^{16}O^{4+}$ from the water vacuum background. Prominent NSI for Ne^{2+}, Ne^{3+}, Ne^{4+}, and Ne^{5+} is apparent in Fig. 1 by the deviation from the SI yield for ion yields $<10^4$ ions/(shot torr). One may see from the yield of Ne^{4+}, NSI exceeds not only the SI yield of the final species, i.e., Ne^{4+}, but also of the preceding charge state Ne^{3+}. Furthermore, at 2×10^{15} W/cm^2, well below the saturation intensity of Ne^{2+}, NSI is prominent in Ne^{3+} and Ne^{4+}. In these studies, electron processes beyond simple $(e, 2e)$ impact ionization or impact excitation of a singly excited state must be involved since the NSI is correlated with SI of the prior two charge states.

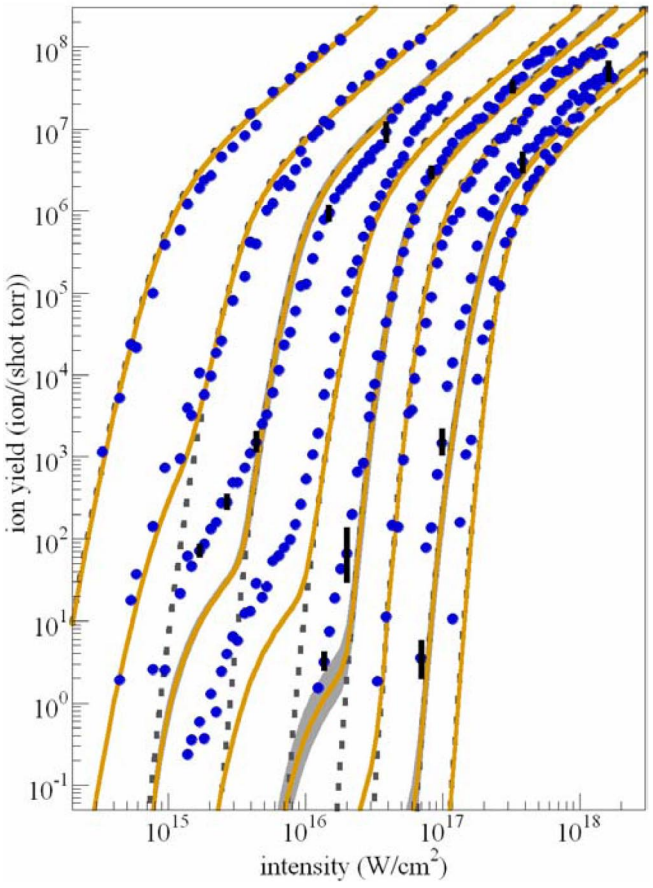

FIG. 1 (color online). Experimental (circles) Ne^+ to Ne^{8+} (left to right) yields with ADK (dashed line) and our calculation (solid line). Data fluctuations (bars) and calculated extremes (shaded) are shown for Ne^{3+}, Ne^{5+}, and Ne^{7+}. Extremes are only slightly larger than the line width for Ne^{3+} and Ne^{7+}.

To calculate NSI, we have used a semiclassical 3D relativistic, rescattering model. In the model we treat the first "step" of the ionization nonrelativistically using ADK. The second rescattering step uses a 3D ensemble of $\sim 10^3$ classical trajectories to model the photoelectron in the continuum whenever the ADK rate is significant. The initial trajectory ensemble coordinates are the outer point of the tunneling barrier with a transverse probability distribution matched to the ADK rate. The ensemble is also given a transverse momentum [25] ($\Delta p_\perp{}^2 = \mathrm{E}_{\text{laser}}/\sqrt{2V_{\text{IP}}}$ in atomic units where V_{IP} is the parent ion ionization potential) so the ensemble spreads in time as expected for a quantum photoelectron. The trajectories are calculated by numerically solving the relativistic equation of motion with the force given by $\mathbf{F} = q(\mathbf{E}_{\text{laser}} + \mathbf{E}_{\text{ion}}) + q\mathbf{v} \times \mathbf{B}_{\text{laser}}$, where $\mathbf{E}_{\text{ion}}$ is the field from a central, soft-core ion potential with charge Z, $V_{\text{ion}}(r) = -Z/\sqrt{r^2 + (Z/2V_{\text{IP}})^2}$.

Figure 2(a) is a trajectory ensemble for the photoionization of Ne^{7+} at 10^{17} W/cm^2. (Only $\sim$50 trajectories are shown projected onto the plane containing $\mathbf{E}_{\text{laser}}$ (x axis) and the propagation direction k (z axis).) In Fig. 2(b) the trajectories are binned to illustrate how the classical trajectory ensemble generates a rescattering flux comparable to a quantum photoelectron. The role of the Lorentz force on the rescattering photoelectron can be seen in Figs. 2(a) and 2(b) when the photoelectron returns to the parent ion ($t = 96$ a.u. in the figure) and has been deflected by 150 a.u. along z. Despite this, the large wave function spread (also of order 150 a.u. in Fig. 2(b)] allows some rescattering to still occur.

The rescattering flux is used with the field free electron impact cross sections to quantify the impact ionization and

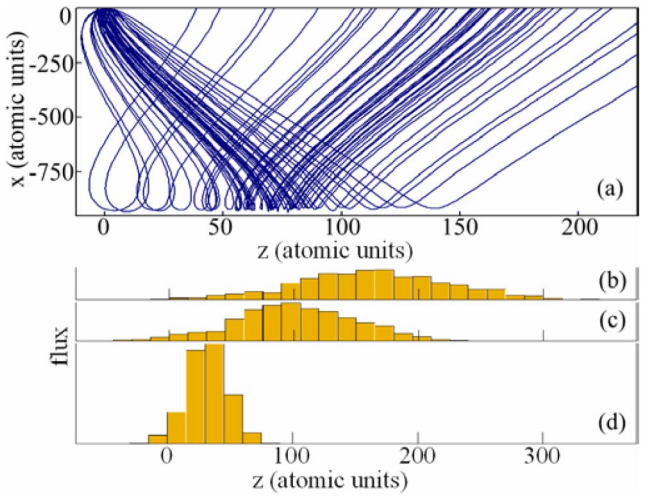

FIG. 2 (color online). Ne^{7+} photoionization trajectory ensemble (a) and flux for $t = 25$ au (d), 75 au (c), and 96 au (b) after ionization.

excitation. We have reduced the available data by fitting to a Lotz's cross section [26] $\sigma = a\ln(E/V_{\mathrm{IP}}) \times (1 - b\exp(-c(E/V_{\mathrm{IP}} - 1))(EV_{\mathrm{IP}})^{-1}$ where a, b, and c are fit parameters. The impact ionization cross sections used in this work are given in Figs. 3(a) and 3(b). For Ne^{2+}, Ne^{3+}, Ne^{4+}, where $(e, 3e)$ cross sections are not known, we scaled available $(e, 3e)$ cross section data from isoelectronic species [27,28] using $\sigma_{\mathrm{Ne}} = f(E/V_{\mathrm{IP,iso}}) \times (V_{\mathrm{IP,iso}}/V_{\mathrm{IP,Ne}})^2$, where σ_{Ne} is the scaled cross section for Ne with a threshold of $V_{\mathrm{IP,Ne}}$ and $f(E/V_{\mathrm{IP,iso}})$ is the cross section of an isoelectronic ion with its energy dependence E scaled to its threshold $V_{\mathrm{IP,iso}}$ [29,30]. Because scaled isoelectronic $(e, 3e)$ cross sections are within 25% of the measured cross sections for Ne^{+}, Ne^{5+}, and Ne^{6+} we believe the scaled Ne^{2+}, Ne^{3+}, and Ne^{4+} cross sections have a similar accuracy [31–34]. Representative error bars are shown in Fig. 3 for several of the cross sections. Use of field free (e, ne) impact ionization cross sections is expected to give an error of less than 20% when compared to cross sections in a strong laser field [35]. Impact excitation cross sections [Figs. 3(c) and 3(d)] used in this study were taken from data for Ne^{4+}, Ne^{6+}, and Ne^{7+} [32]. Ne^{+}, Ne^{2+}, Ne^{3+} and Ne^{5+} excitation cross sections were obtained by scaling isoelectronic cross sections of nearby species O, P, C, N, and Al [32,36–38]. The largest excitation cross sections from the ion ground states were included in this study: Ne^{+} ($2s^1 2p^{62}$S, $2s^2 2p^4 3s^2$P, and ^{4}P), Ne^{2+} ($2s^1 2p^{53}$P and $2s^2 2p^3 3s^3$S, $2p^6$), Ne^{3+} ($2s^1 2p^{44}$P, $2s^2 2p^2 3s^4$P, and $2p^{52}$P), Ne^{4+} ($2s2p^{33}$P and ^{3}S, $2p^{43}$P), Ne^{5+} ($2s2p^{22}$P and ^{2}D, $2s^2 3d^2$D, $2p^{32}$D, and ^{2}P), Ne^{6+} ($2s2p^1$P, $2s3d^1$P, and $2p^{21}$D), and Ne^{7+} ($2p^2$P, $3d^2$D). Excitation is included in the model under the assumption it leads to prompt ionization.

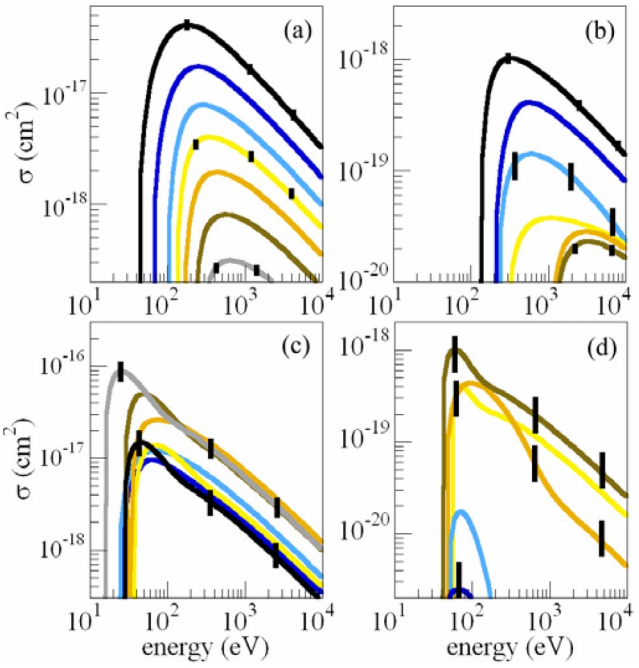

FIG. 3 (color online). Impact cross sections for $(e, 2e)$ (a) and $(e, 3e)$ (b) ionization along with single-excitation (c) and double-excitation (d). Initial states are [top to bottom in panel (a)] Ne^{2+} (black), Ne^{3+} (blue), Ne^{4+} (light blue), Ne^{5+} (yellow), Ne^{6+} (dark yellow), Ne^{7+} (brown), and Ne^{8+} (gray).

Our calculated total ionization yield, including SI and rescattering NSI, is shown in Fig. 1. For the double ionization of Ne, the model accounts for the observed NSI and SI (Fig. 1). This result can be compared to studies of He [15] where a similar physical model has been able to reproduce NSI. For higher ionization processes Ne^{3+} and Ne^{4+} our model accounts for 15% of the measured NSI, i.e., a seven-fold under representation of NSI from 2×10^{15} W/cm^2 to 3×10^{15} W/cm^2. For higher charge states, $(e, 3e)$ and doubly excited states give rise to a larger component of NSI than $(e, 2e)$ ionization and one-electron excitation processes. Because NSI for Ne^{3+} and Ne^{4+} follows the Ne^{+} and Ne^{2+} yields, respectively, the most probable explanation requires an additional doubly excited state mechanism, such as rescattering ionization of an atom with trapped population in Rydberg states [39] ($Ne + n\hbar\omega \rightarrow Ne^{+*} + e^- + n'\hbar\omega \rightarrow Ne^{+3} + 3e^-$ where Ne^{+*} is excited state Ne^{+}), or "chain" rescattering of NSI ($Ne + n\hbar\omega \rightarrow Ne^{+} + e^- + n'\hbar\omega \rightarrow Ne^{+2} + 2e^- + n''\hbar\omega \rightarrow Ne^{+3} + 3e^-$), which are not included in our model.

For Ne^{5+}, the difference between experiment and theory varies and the agreement is good for NSI yields near 1 ion/shot torr in Fig. 1. NSI of Ne^{5+} and Ne^{6+} is near the transition point ($\sim 3 \times 10^{16}$ W/cm^2) between the strong and ultrastrong field and additional dynamics involving $\mathbf{B}_{\mathrm{laser}}$ may play a role. As the intensity is increased, NSI may be at the edge of the experimental sensitivity for Ne^{6+}. NSI is not observed in Ne^{7+} or Ne^{8+}. In our calculations, NSI in Ne^{8+} is 10^{-9} of the SI yield at saturation.

The lack of measured cross sections and uncertainties among existing data makes it more difficult to accurately model Ne than, for example, He. The maximum and minimum extreme yield from the calculation due to cross section uncertainties and experimental fluctuations are shown in Fig. 1 as a shaded region for Ne^{3+}, Ne^{5+}, and Ne^{7+}. The maximum was calculated using a 60 fs pulse and the largest cross section allowed by the error bars (Fig. 2). The minimum was calculated using a 25 fs pulse and the smallest cross section allowed. The discrepancies between the model and NSI in Ne^{3+}, Ne^{4+}, and Ne^{5+} cannot be explained by these uncertainties.

One of the outstanding questions in ultrastrong fields is, "When is $\mathbf{B}_{\mathrm{laser}}$ a significant part of the excitation or ionization physics?" Fig. 4(b) presents the results of our calculation with and without $\mathbf{B}_{\mathrm{laser}}$. One can conclude from Fig. 4 that NSI for Ne^{7+} and Ne^{8+} will be overestimated if one ignores $\mathbf{B}_{\mathrm{laser}}$. Above 10^{17} W/cm^2, the difference due to the magnetic field is expected to be an order of magnitude for Ne^{8+}. However, the calculated Ne^{6+} yields at 2×10^{16} W/cm^2 with or without $\mathbf{B}_{\mathrm{laser}}$ are equivalent. This

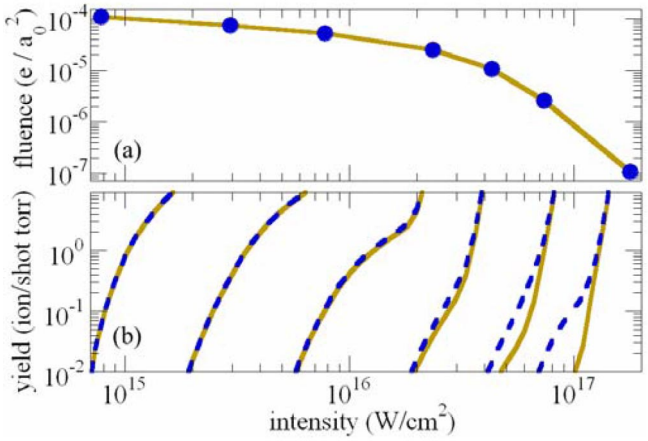

FIG. 4 (color online). Ne^+ to Ne^{7+} rescattering fluence (a) and Ne^{3+} to Ne^{8+} yields (b) calculated with (solid line) and without (dashed line) $\mathbf{B}_{\text{laser}}$.

means the decrease in the NSI due to rescattering observed in Fig. 1 below 10^{16} W/cm^2 is due primarily to the decrease in the collision cross sections shown in Fig. 3 and not $\mathbf{B}_{\text{laser}}$.

The decrease of (e, ne) NSI at 10^{17} W/cm^2 due to $\mathbf{B}_{\text{laser}}$ is the result of the Lorentz deflection of the rescattering. Figure 4(a) shows the decrease in the rescattering flux at the parent ion nucleus (origin) as a function of intensity in absolute units. The calculation was done at the saturation intensity for the Ne charge states. In Fig. 4(a), the rescattering flux significantly drops above 3×10^{16} W/cm^2. This decrease in rescattering should also become apparent in HHG beyond 3×10^{16} W/cm^2.

In conclusion, as one moves from the strong field into the ultrastrong field regime the NSI in Ne decreases by 10^4. The yields of Ne^+ and Ne^{2+} are well represented by a model using an ADK ionization rate for SI and impact ionization and excitation cross sections for NSI. Ne^{3+}, Ne^{4+}, and Ne^{5+} ionization yields require interactions beyond $(e, 2e)$, $(e, 3e)$ and impact excitation of primary single- and double-excited states. An additional doubly excited state or chain NSI rescattering mechanism is required to explain the increased yields of NSI in Ne^{3+} and Ne^{4+}. The experimental yields of Ne^{7+} and Ne^{8+} agree with a sequential ADK model over the dynamic range. The decrease in the NSI yield from Ne^{2+} to Ne^{8+} is primarily the result of smaller impact cross sections for higher charged ion states. Our calculations indicate the Lorentz deflection of the photoelectron will begin to suppress rescattering at intensities of 10^{17} W/cm^2.

This material is based upon work supported by the National Science Foundation under Grant No. 0140331.

[1] C. Ruiz, L. Plaja, and L. Roso, Phys. Rev. Lett. **94**, 063002 (2005).
[2] P. J. Ho, R. Panfili, S. L. Haan, and J. H. Eberly, Phys. Rev. Lett. **94**, 093002 (2005).
[3] H. Niikura, D. M. Villeneuve, and P. B. Corkum, Phys. Rev. Lett. **94**, 083003 (2005).
[4] R. Lopez-Marens *et al.*, Phys. Rev. Lett. **94**, 033001 (2005).
[5] L. F. DiMauro and P. Agostini, in *Ionization Dynamics in Strong Laser Fields*, edited by B. Bederson and H. Walther, Adv. At. Mol. Opt. Phys. Vol. 35 (Academic Press, San Diego, Calif., 1995).
[6] A. Rundquist *et al.*, Science **280**, 1412 (1998).
[7] P. B. Corkum, Phys. Rev. Lett. **71**, 1994 (1993).
[8] B. Walker *et al.*, Phys. Rev. Lett. **73**, 1227 (1994).
[9] Andreas Becker and Farhad H. M. Faisal, J. Phys. B **29**, L197 (1996).
[10] H. W. van der Hart and K. Burnett, Phys. Rev. A **62**, 013407 (2000).
[11] M. Lein, E. K. U. Gross, and V. Engel, Phys. Rev. Lett. **85**, 4707 (2000).
[12] R. Kopold *et al.*, Phys. Rev. Lett. **85**, 3781 (2000).
[13] J. Rudati *et al.*, Phys. Rev. Lett. **92**, 203001 (2004).
[14] B. Walker *et al.*, Phys. Rev. A **48**, R894 (1993).
[15] G. L. Yudin and M. Y. Ivanov, Phys. Rev. A **63**, 033404 (2001).
[16] S. Larochelle, A. Talebpour, and S. L. Chin, J. Phys. B **31**, 1201 (1998).
[17] M. Weckenbrock *et al.*, Phys. Rev. Lett. **92**, 213002 (2004).
[18] R. Moshammer *et al.*, Phys. Rev. Lett. **84**, 447 (2000).
[19] A. Rudenko *et al.*, Phys. Rev. Lett. **93**, 253001 (2004).
[20] E. A. Chowdhury and B. C. Walker, J. Opt. Soc. Am. B **20**, 109 (2003).
[21] M. Dammasch *et al.*, Phys. Rev. A **64**, 061402 (2001).
[22] J. Yang and B. C. Walker, Opt. Lett. **26**, 453 (2001).
[23] A. DiChiara *et al.*, Opt. Lett. **28**, 2106 (2003).
[24] M. V. Ammosov, N. B. Delone, and V. P. Krainov, Sov. Phys. JETP **64**, 1191 (1986).
[25] N. B. Delone and V. P. Krainov, J. Opt. Soc. Am. B **8**, 1207 (1991).
[26] W. Lotz, Z. Phys. **216**, 241 (1968).
[27] M. Westerman *et al.*, Phys. Scr. **T80B**, 285 (1999).
[28] W. R. Thompson, M. B. Shah, and H. B. Gilbody, J. Phys. B **28**, 1321 (1995).
[29] M. Gryzinski and J. A. Kunc, J. Phys. B **19**, 2479 (1986).
[30] A. V. Eletskii and B. M. Smirnov, Sov. Phys. Tech. Phys. **13**, 1 (1968).
[31] D. P. Almeida, A. C. Fontes, and C. F. L. Godinho, J. Phys. B **28**, 3335 (1995).
[32] NIFS Bibliographic and Numerical Atomic & Molecular Databases, http://dbshino.nifs.ac.jp/.
[33] M. Zambra, D. Belic, P. Defrance, and D. J. Yu, J. Phys. B **27**, 2383 (1994).
[34] M. Duponchelle *et al.*, J. Phys. B **30**, 729 (1997).
[35] K. C. Kulander, J. Cooper, and K. J. Schafer, Phys. Rev. A **51**, 561 (1995).
[36] I. Kanik *et al.*, J. Phys. B **34**, 2647 (2001).
[37] M. E. Bannister *et al.*, Int. J. Mass Spectrom. **192**, 39 (1999).
[38] J. A. Lozano *et al.*, Phys. Rev. A **63**, 042713 (2001).
[39] R. R. Jones, D. W. Schumacher, and P. H. Bucksbaum, Phys. Rev. A **47**, R49 (1993).